Determining the Equivalent Impedance Boundary Condition for Corrugated Coatings Based on the Genetic Algorithm

Tao Su, *Student Member, IEEE,* and Hao Ling

***Abstract*—A methodology based on the genetic algorithm (GA) is proposed to determine the equivalent impedance boundary condition (IBC) for corrugated material coating structures. In this approach, rigorous solutions of the reflection coefficients at a number of incident angles are first calculated using a periodic method of moments (MoM) solver. The IBC model is used to predict the reflection coefficients at the same observation angles. The model coefficients are then optimized using the GA so that the difference between the approximated and the MoM predicted reflection coefficients is minimized. The GA proves efficient in obtaining an optimal IBC model. The resulting IBC model can be readily incorporated into an existing computational electromagnetics code to assess the performance of the corrugated coating when mounted on complex platforms.**

***Index Terms*—Coatings, genetic algorithm, gratings, impedance boundary conditions.**

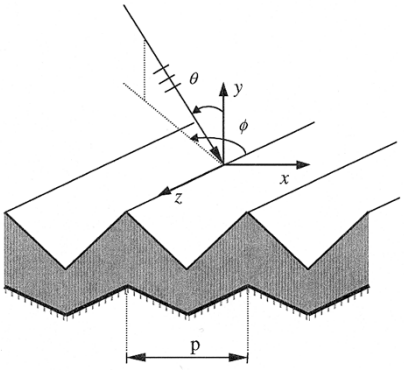

Fig. 1. Scattering from a corrugated coating structure backed by a conducting surface.

I. Introduction

IT is well known that the impedance boundary condition (IBC) approximation is an efficient way to model complex structures such as material coatings and subskinline features [1]–[3]. It replaces the original volumetric structure with a surface impedance so that the problem dimension is reduced by one. Thus, large savings in computational resources can be achieved in the analysis of the original problem. However, to determine a simple IBC for an arbitrary structure that is valid over a wide range of incident angles, polarizations and frequencies is a nontrivial task. In this paper, we set out to develop a methodology to determine the equivalent IBC model for a corrugated coating structure backed by a conducting surface (see Fig. 1). The corrugation of the surface is assumed to be periodic in one dimension along the x-axis. Of interest is an IBC model that is valid over a large range of incident angles in both the θ and ϕ directions. Our objective is to establish a robust methodology such that the resulting IBC model can be used in place of the actual coating structure in subsequent analysis and design involving complex platforms.

The problem at hand is difficult since the scattering characteristics of the corrugated surface is strongly dependent on polarization and incident angle. The standard IBC used for flat coatings accounts for neither the aniostropic nor the angular behavior of the scattering characteristics of the corrugated surface. Some improved impedance boundary conditions have been proposed in the literature, including the tensor impedance boundary condition (TIBC) [1] and the generalized impedance boundary condition (GIBC) [2], [4]. TIBC usually works only for a very limited range of incident angles. GIBC improves the accuracy of the IBC model by including higher order derivatives of the fields on the surface. However, it cannot be easily implemented in existing MoM solvers since it requires further reformulation in the integral equation. A resistive boundary condition (RBC) has been reported that works well over large incident angles for two-dimensional (2-D) planar periodic surfaces [5]. However, it is limited to surfaces with very small periods. Furthermore, the choice for the position of the equivalent impedance surface is not obvious for the corrugated structure.

Our proposed approach to this problem is based on the genetic algorithm (GA). First, we compute the reflection coefficients from the corrugated surface over a number of incident angles and polarizations using a periodic method of moments (MoM) solver [6]. The resulting reflection coefficients constitute our reference data base. Next, a simple periodic IBC model is proposed from which we can derive an expression for the reflection coefficients. In the GA step, we optimize the model coefficients so that the difference between the IBC-predicted and the MoM-predicted reflection coefficients is minimized. GA searches the entire parameter space in a way similar to natural evolution and arrives, after many generations, at the best parameters for the model.

Manuscript received May 26, 1998; revised August 10, 1999. This work was supported by a Lockheed Martin Cooperation Research Grant; in part by the Air Force MURI Center for Computational Electromagnetics under Contract AFOSR F49620-96-1-0025; and in part by the Office of Naval Research under Contract N00014-98-1-0178.

The authors are with the Department of Electrical and Computer Engineering, University of Texas at Austin, Austin, TX 78712 USA.

Publisher Item Identifier S 0018-926X(00)02452-2.

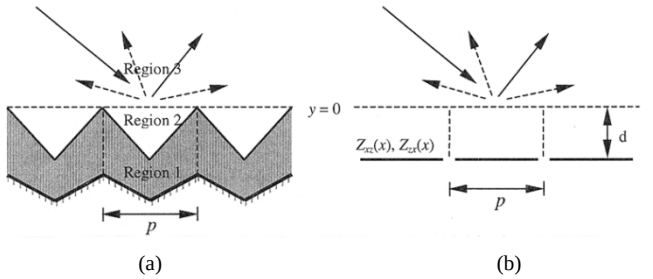

(a) (b)

Fig. 2. Equivalent impedance boundary problem, (a) Original structure, (b) IBC Approximation.

This paper is organized as follows. In Section II, the MoM solution of the problem, the IBC model formulation and the GA optimization are discussed as the steps of the IBC determination. Numerical results are provided in Section III to verify the effectiveness of the approach in a number of corrugated geometries. A 3-D scattering example is also given to demonstrate the utility of the resulting IBC model.

II. Methodology for Determining the Optimal IBC Model

In this section, we describe the proposed methodology for determining the equivalent IBC of a corrugated coating using the GA. In the first step, the reflection coefficients from the coating are computed using the MoM at multiple incident angles to serve as the reference data of the model. The MoM solution for the corrugated coating structure in Fig. 1 has been formulated earlier in [6]. The formulation entails dividing one cell of the grating into different homogeneous regions according to the material layers as shown in Fig. 2(a). Boundary integral equations are first obtained for each region. Field continuity at region interfaces and periodic boundary conditions at cell boundaries are then enforced. The fields in the top half-space are expanded into a sum of Floquet harmonics and are matched to the fields in the lower region so that the reflection coefficients can be found.

In the next step, a periodic IBC model is proposed, from which we can derive an expression for the reflection coefficients. In the final step, the optimal parameters for the IBC model are obtained by minimizing the mean squared error between the two sets of reflection coefficients based on the GA. These steps are described in detail below.

A. Periodic IBC Model

The equivalent IBC relating the tangential electric and magnetic fields for a planar coated surface can be written as [1]:

$$\begin{bmatrix} E_z \\ E_x \end{bmatrix} = \begin{bmatrix} Z_{zz} & Z_{zx} \\ Z_{xz} & Z_{xx} \end{bmatrix} \begin{bmatrix} H_z \\ H_x \end{bmatrix} \tag{1}$$

We shall adopt this model for the corrugated problem due to its simplicity and usefulness for our applications. The model parameters will then be optimized to emulate the properties of the exact structure. Note that since the corrugated surface exhibits anisotropic scattering characteristics, the equivalent IBC must also in general be anisotropic. Therefore, the cross impedance terms Z_{xx} and Z_{zz} are kept in our formulation to assess their importance. The boundary impedance Z_{zz}, Z_{zx}, Z_{xz}, and Z_{xx} are

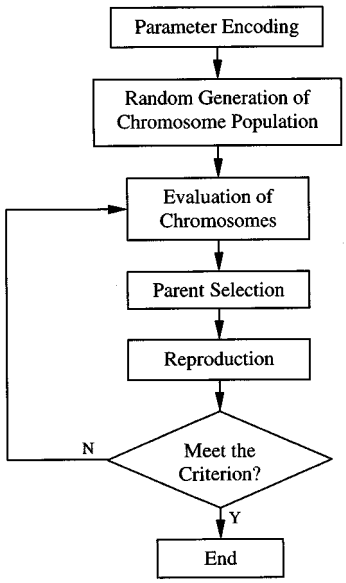

Fig. 3. Flow chart of the GA.

in general functions of incident angle and spatial position. For the IBC model to be useful for subsequent electromagnetic analysis, however, it is much preferable to model the boundary impedances as functions of spatial position only. We cannot prove theoretically the existence of such a model for an arbitrary corrugated structure. Instead, the applicability and limitation of this approach will be explored numerically in Section III.

In our IBC model, the periodic grating structure with period p, as shown in Fig. 2(a), is replaced by an equivalent impedance boundary condition, which also has a period p, as illustrated in Fig. 2(b). Each surface impedance term can be expanded into a Fourier series. Since the cross impedance terms Z_{zz} and Z_{xx} are usually very small, we shall treat them as constants and only expand the impedances Z_{zx} and Z_{xz} as

$$Z_{zx} = \sum_{n=-\infty}^{\infty} a_n e^{-j\frac{2\pi}{p}nx}, \quad Z_{xz} = \sum_{n=-\infty}^{\infty} b_n e^{-j\frac{2\pi}{p}nx}. \tag{2}$$

Therefore, to fully describe the IBC model, we must determine the Fourier series coefficients $\{a_n\}$ and $\{b_n\}$.

B. Solution to the Forward Problem of Scattering by the IBC Model

Next, we derive the reflection coefficients resulting from the plane wave scattering from the IBC model given above. Under plane wave incidence where

$$k_{x0}^i = k_0 \sin\theta \sin\phi, \quad k_{y0}^i = -k_0 \cos\theta \quad \text{and}$$
$$k_{z0}^i = k_0 \sin\theta \cos\phi$$

each component of the tangential electric and magnetic fields at the impedance surface can be expanded into a sum of Floquet harmonics [7]. For example, the tangential electric field in the z direction is expanded as

$$E_z = E_z^i e^{-jk_{x0}x} + \sum_{n=-\infty}^{\infty} E_{zn}^r e^{-jk_{xn}x} \tag{3}$$

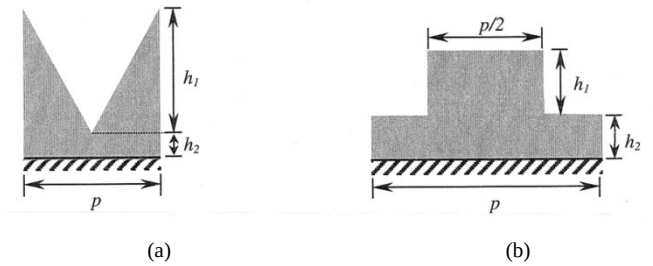

(a) (b)

Fig. 4. Grating geometry for (a) triangular groove and (b) rectangular groove.

where

$$k_{xn} = k_{x0} + n\frac{2\pi}{p}$$

is the propagation constant of the nth order harmonic along the x-direction. This Floquet harmonic is a reflected wave with propagation constants (k_{xn}, k_{yn}^r, k_z), where $k_{yn}^r = \sqrt{k_0^2 - k_z^2 - k_{xn}^2}$ with the square root taken as positive real or negative imaginary. The superscripts i and r denote respectively the incident and reflected field throughout this paper. The harmonic term $e^{j\omega t}e^{-jk_z z}$ is suppressed in (3) and y is set to zero at the impedance surface for convenience. Assuming that the coefficients of the higher order Floquet harmonics are negligible and applying this to other tangential field components we get

$$F = F^i e^{-jk_{x0}x} + \sum_{n=-N}^{N} F_n^r e^{-jk_{xn}x} \tag{4}$$

where F can be E_z, H_z, E_x or H_x, and N is a positive integer. Substituting (2) and (4) into (1) and matching the coefficients of the exponential terms, we obtain a set of equations relating E_{zn}, H_{xn} and H_{zn}

$$E_z^i\delta_{n0} + E_{zn}^r = Z_{zz}H_{zn}^r + \sum_{m=-N}^{N} a_{n-m}H_{xm}^r + a_n H_x^i + Z_{zz}H_z^i\delta_{n0} \tag{5}$$

for $n = -N$ to N. δ_{n0} is the Kronecker delta. This set of equations can be written in matrix form as

$$E_z^i\mathbf{u}_N + \mathbf{E}_z^r = Z_{zz}\mathbf{H}_z^r + \mathbf{A}\mathbf{H}_x^r + H_x^i\mathbf{a} + Z_{zz}H_z^i\mathbf{u}_N \tag{6}$$

where

$$\mathbf{E}_z^r = [E_{z,-N}^r \quad \cdots \quad E_{z0}^r \quad \cdots \quad E_{z,N}^r]^{\mathbf{T}}$$
$$\mathbf{H}_z^r = [H_{z,-N}^r \quad \cdots \quad H_{z0}^r \quad \cdots \quad H_{z,N}^r]^{\mathbf{T}}$$
$$\mathbf{H}_x^r = [H_{x,-N}^r \quad \cdots \quad H_{x0}^r \quad \cdots \quad H_{x,N}^r]^{\mathbf{T}}$$

$$\mathbf{A} = \begin{bmatrix} a_0 & \cdots & a_{-N} & \cdots & a_{-2N} \\ \vdots & \ddots & \vdots & \ddots & \vdots \\ a_N & \cdots & a_0 & \cdots & a_{-N} \\ \vdots & \ddots & \vdots & \ddots & \vdots \\ a_{2N} & \cdots & a_N & \cdots & a_0 \end{bmatrix}, \quad \mathbf{a} = \begin{bmatrix} a_{-N} \\ \vdots \\ a_0 \\ \vdots \\ a_N \end{bmatrix}$$

and

$$\mathbf{u}_N = [u_{-N} \quad \cdots \quad u_0 \quad \cdots \quad u_N]^{\mathbf{T}}, \quad u_n = \delta_{n0}.$$

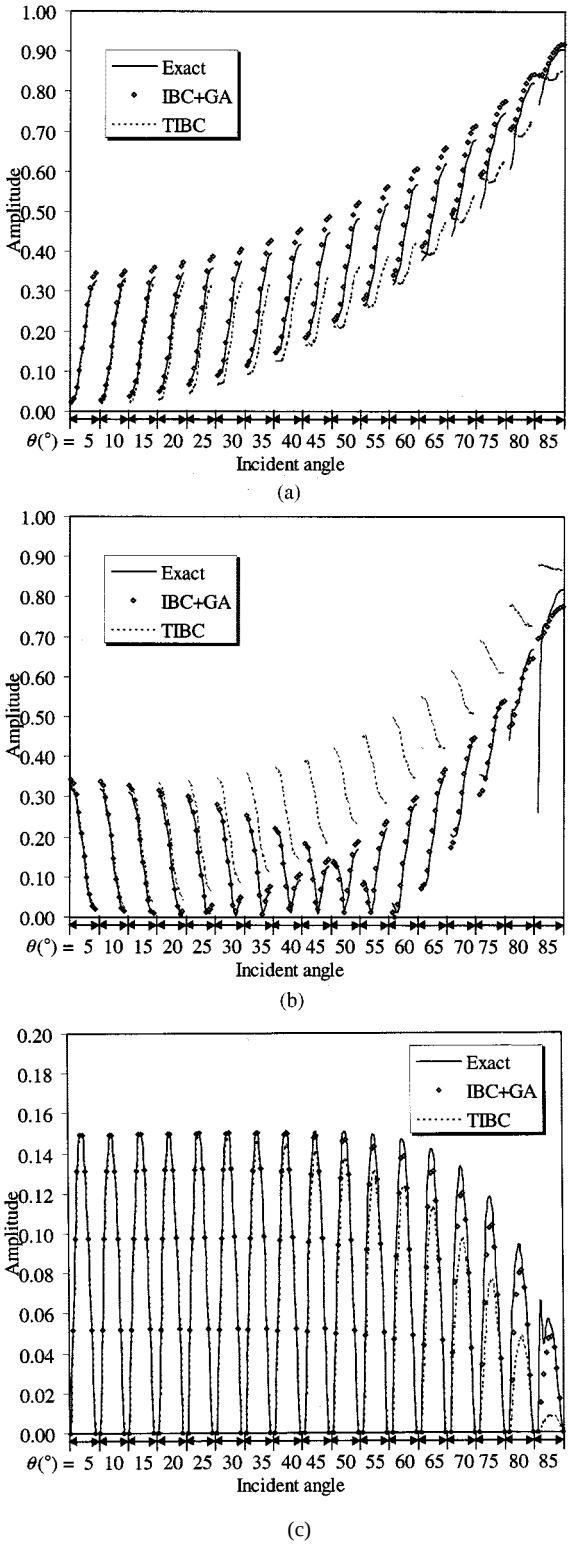

Fig. 5. Comparison of reflection coefficients versus angle among: 1) the exact MOM result; 2) the IBC derived from GA; and 3) the TIBC result. (a) H-polarization. (b) V-polarization. (c) H–V cross polarization.

Following the same steps, we also arrive at the relationship for E_{xn}, H_{xn}, and H_{zn}

$$\mathbf{B}\mathbf{H}_z^r = \mathbf{E}_x^r - Z_{xx}\mathbf{H}_x^r + E_x^i\mathbf{u}_N - Z_{xx}H_x^i\mathbf{u}_N - H_z^i\mathbf{b} \tag{7}$$

where

$$\mathbf{B}=\begin{bmatrix} b_0 & \cdots & b_{-N} & \cdots & b_{-2N} \\ \vdots & \ddots & \vdots & \ddots & \vdots \\ b_N & \cdots & b_0 & \cdots & b_{-N} \\ \vdots & \ddots & \vdots & \ddots & \vdots \\ b_{2N} & \cdots & b_N & \cdots & b_0 \end{bmatrix}, \quad \mathbf{b}=\begin{bmatrix} b_{-N} \\ \vdots \\ b_0 \\ \vdots \\ b_N \end{bmatrix}.$$

For a plane wave, the tangential components of the fields in the x-direction E_x, H_x can be expressed in terms of E_z and H_z as

$$\begin{bmatrix} \mathbf{E}_x^r \\ \mathbf{H}_x^r \end{bmatrix}=[\mathbf{T}]\begin{bmatrix} \mathbf{E}_z^r \\ \mathbf{H}_z^r \end{bmatrix}, \quad \text{and} \quad \begin{bmatrix} E_x^i \\ H_x^i \end{bmatrix}=[\mathbf{T}^i]\begin{bmatrix} E_z^i \\ H_z^i \end{bmatrix} \tag{8}$$

where

$$\mathbf{T}=\begin{bmatrix} -\frac{k_{x,-N}k_z}{k_t^2} & 0 & -\frac{k_{y,-N}^r k_0}{k_t^2}\eta_0 & 0 \\ & \ddots & & \ddots \\ 0 & -\frac{k_{xN}k_z}{k_t^2} & 0 & -\frac{k_{yN}^r k_0}{k_t^2}\eta_0 \\ \frac{k_{y,-N}^r k_0}{k_t^2\eta_0} & 0 & -\frac{k_{x,-N}k_z}{k_t^2} & 0 \\ & \ddots & & \ddots \\ 0 & \frac{k_{yN}^r k_0}{k_t^2\eta_0} & 0 & -\frac{k_{xN}k_z}{k_t^2} \end{bmatrix}$$

and

$$\mathbf{T}^i=\begin{bmatrix} -\frac{k_{x0}k_z}{k_t^2} & -\frac{k_{y0}^i k_0}{k_t^2}\eta_0 \\ \frac{k_{y0}^i k_0}{\eta_0 k_t^2} & -\frac{k_{x0}k_z}{k_t^2} \end{bmatrix}, \quad \left(k_t=\sqrt{k_0^2-k_z^2}\right).$$

Combine (6)–(8), the matrix relationship between the incident and reflected fields is written as

$$\begin{aligned}\begin{bmatrix} \mathbf{E}_z^r \\ \mathbf{H}_z^r \end{bmatrix}=&\left(\begin{bmatrix} \mathbf{I} & -Z_{zz}\mathbf{I} \\ 0 & \mathbf{B} \end{bmatrix}-\begin{bmatrix} 0 & \mathbf{A} \\ \mathbf{I} & -Z_{xx}\mathbf{I} \end{bmatrix}[\mathbf{T}]\right)^{-1} \\ &\times\left(\begin{bmatrix} 0 & \mathbf{a} \\ \mathbf{u}_N & -Z_{zz}\mathbf{u}_N \end{bmatrix}[\mathbf{T}^i]+\begin{bmatrix} -\mathbf{u}_N & -Z_{xx}\mathbf{u}_N \\ 0 & \mathbf{b} \end{bmatrix}\right) \\ &\times\begin{bmatrix} E_z^i \\ H_z^i \end{bmatrix}.\end{aligned} \tag{9}$$

In (9), the z components of the scattered field can be directly related to those of the incident field. We can therefore define the reflection coefficients for the different polarizations as

$$\begin{aligned} R_n^{\mathrm{TM-TM}}&=\left.\frac{E_{zn}^r}{E_z^i}\right|_{H_z^i=0}, & R_n^{\mathrm{TM-TE}}&=\left.-\frac{\eta_0 H_{zn}^r}{E_z^i}\right|_{H_z^i=0} \\ R_n^{\mathrm{TE-TE}}&=\left.-\frac{H_{zn}^r}{H_z^i}\right|_{E_z^i=0}, & R_n^{\mathrm{TE-TM}}&=\left.\frac{E_{zn}^r}{\eta_0 H_z^i}\right|_{E_z^i=0}. \end{aligned} \tag{10}$$

To summarize, the reflection coefficients from the IBC model can be calculated by using (9) and (10) if a_n and b_n are given. This relationship is utilized by the GA to calculate the reflection coefficients for a given sample of $\{a_n\}$ and $\{b_n\}$ and compare them with the reference data obtained from the MoM solution to optimize the model parameters.

Two comments are in order. First, although the reflection coefficients are derived for the $\mathrm{TE}_z/\mathrm{TM}_z$ polarizations, they can be easily transformed to the more conventional vertical (V)/horizontal (H) polarizations with respect to the surface. Second, we have assumed the position of the IBC surface is at $y=0$ in the above formulation. However, if the IBC surface is at the position $y=-d$ [as shown in Fig. 2(b)], a factor of $e^{-j2k_y d}$ should be multiplied to each of the reflection coefficients to arrive at the correct answer. It is well known that in general layered coating problems, there is not a preferred position for the impedance surface. The solution can sometimes be improved by applying the IBC at a position other than a natural interface in the structure [4]. Therefore, by including the position of the IBC surface as an additional tuning parameter in our IBC model, we can further improve the accuracy of the model.

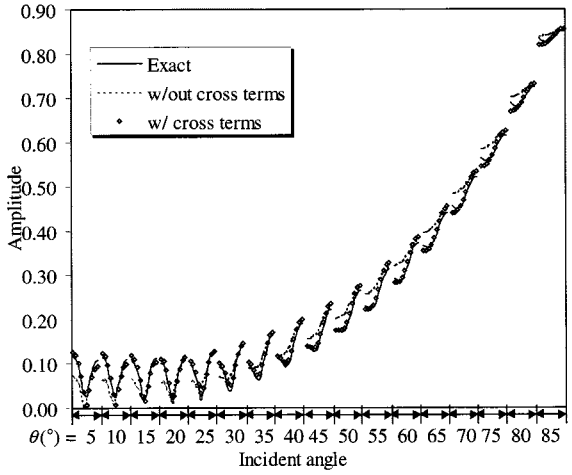

(a)

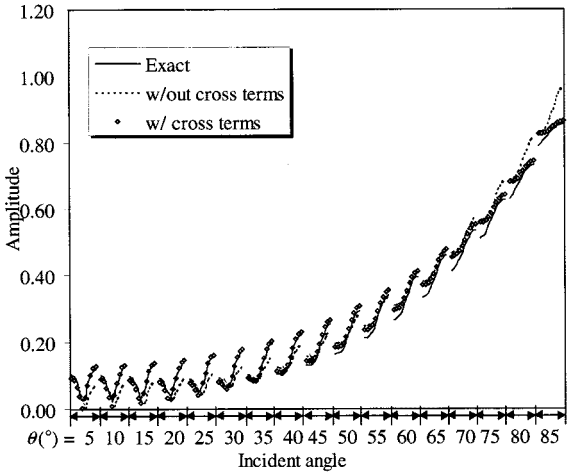

(b)

Fig. 6. Effect of incorporating the cross impedance terms in the IBC model generated from GA, (a) H-polarization, (b) V-polarization.

C. Genetic Algorithm to Determine the Optimal IBC Parameters

In the GA, the parameters to be optimized are first encoded into binary form. A set of the encoded parameters is known as a chromosome. The basic idea of GA is to generate a pool of chromosomes, discard the bad ones, keep the best ones and let them evolve to produce better chromosomes. The evaluation of each chromosome is performed by a cost function which, in this case, is chosen to be the mean-squared error between the MoM computed reflection coefficients and those solved using (9) and (10) with the $(Z_{zz}, a_n, b_n, Z_{xx}, d)$ parameters decoded from the corresponding chromosome. Chromosomes in the pool are ranked according to the cost function. The best ones are selected in pairs

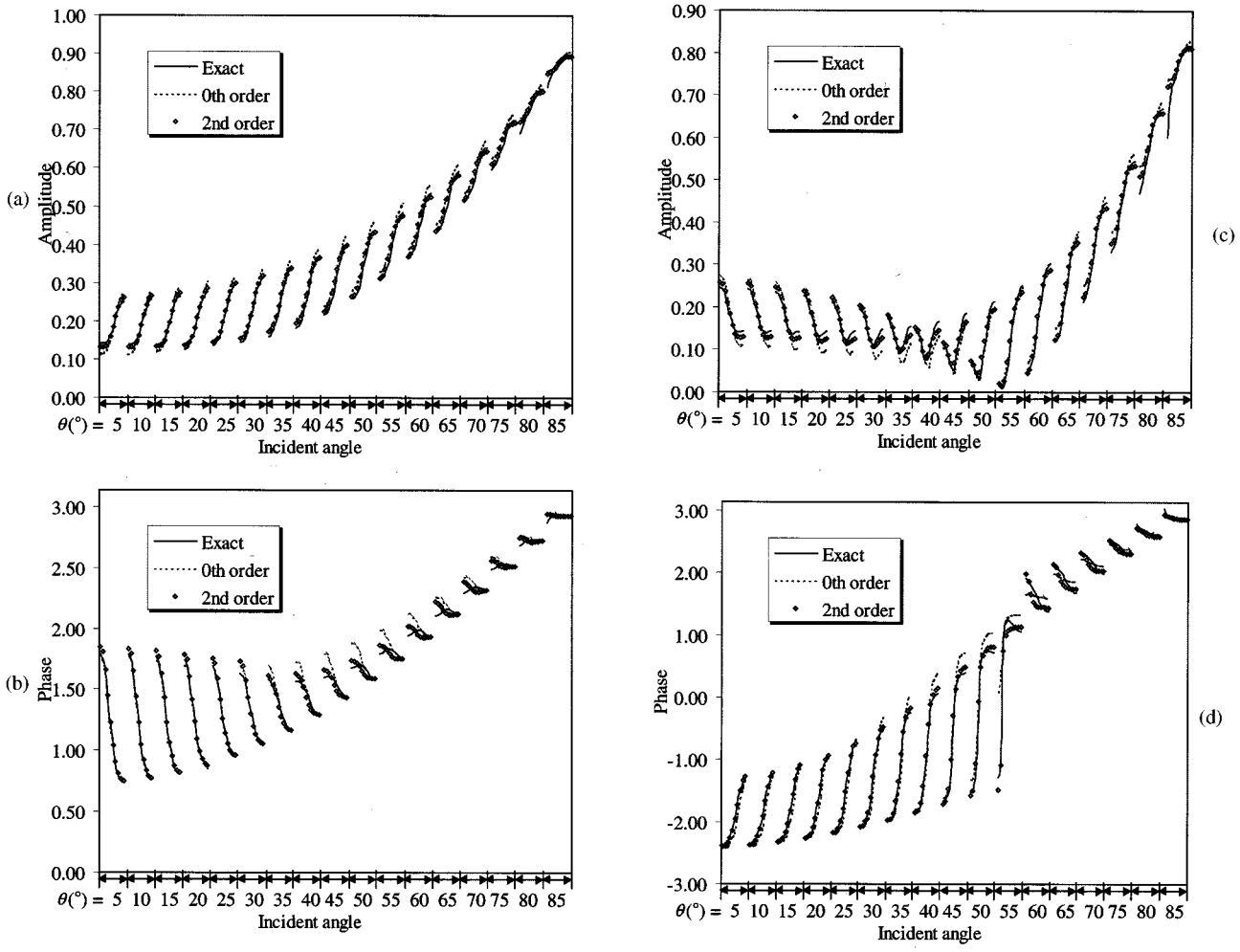

Fig. 7. Effect of increasing the model order in the IBC model generated from GA. (a) Amplitude, H-polarization. (b) Phase, H-polarization. (c) Amplitude, V-polarization. (d) Phase, V-polarization.

to act as parents of the next generation. Reproduction of children chromosomes is based on specific rules of heredity and mutation. The process of selection and reproduction is repeated until a set of satisfactory parameters is found or the generation limit is reached. The flow chart of the GA is shown in Fig. 3. Detailed discussion of the GAs can be found in [8].

In the IBC model for the corrugated coating, the parameters to be optimized are the coefficients of the Fourier expansion a_n and b_n, the cross impedances Z_{zz}, Z_{xx} and the position of the impedance surface d. Each of the parameters a_n, b_n, Z_{zz} and Z_{xx} consists of a real part and an imaginary part. We assume a symmetric structure so that $a_n = a_{-n}, b_n = b_{-n}$. For an approximation truncated to the Nth order, the total number of real numbers is $4N + 9$. The number of bits contained in each parameter B is adjustable. If B is too large, the convergence of GA will be slow. If B is too small, the accuracy of the calculation will suffer. In the examples given in this paper, we choose $B = 8$ to be efficient in both speed and accuracy. In order to encode the unknown parameters into binary form, the minimum and maximum possible values of each parameter are required. For example, the values for the real and imaginary parts of the Fourier series a_n and b_n are estimated to be in the range from $-3\eta_0$ to $3\eta_0$, which is found to be reasonable in the numerical examples. Thus, the eight-bit binary 00000000 denotes $-3\eta_0$ and 11111111 represents $3\eta_0$. Z_{zz} and Z_{xx} are relatively small and their real and imaginary parts vary from $-0.1\eta_0$ to $0.1\eta_0$. The distance d is limited between the upper and lower boundaries of the coating so that the resulting IBC model will not cause any ambiguity in its applications.

In the beginning of the GA, a number of chromosomes are randomly generated. Each chromosome is decoded into parameters Z_{zz}, a_n, b_n, Z_{xx} and d. The reflection coefficients are then computed using (9) and (10). The cost function gives the mean-squared error between these reflection coefficients and their corresponding MoM solution

$$\text{Cost} = \sum_{\theta,\phi} \sum_{P_1,P_2} \left| R^{P_1-P_2} - R_0^{P_1-P_2} \right|^2$$

where R_0 denotes the MoM solution of the reflection coefficients at a specific observation angle (θ, ϕ) and P_1, P_2 is the polarization TE_z/TM_z (or V/H). The fitness value of each chromosome is given by

$$f(C_i) = c_1 - c_2 \,\text{Cost}(C_i)$$

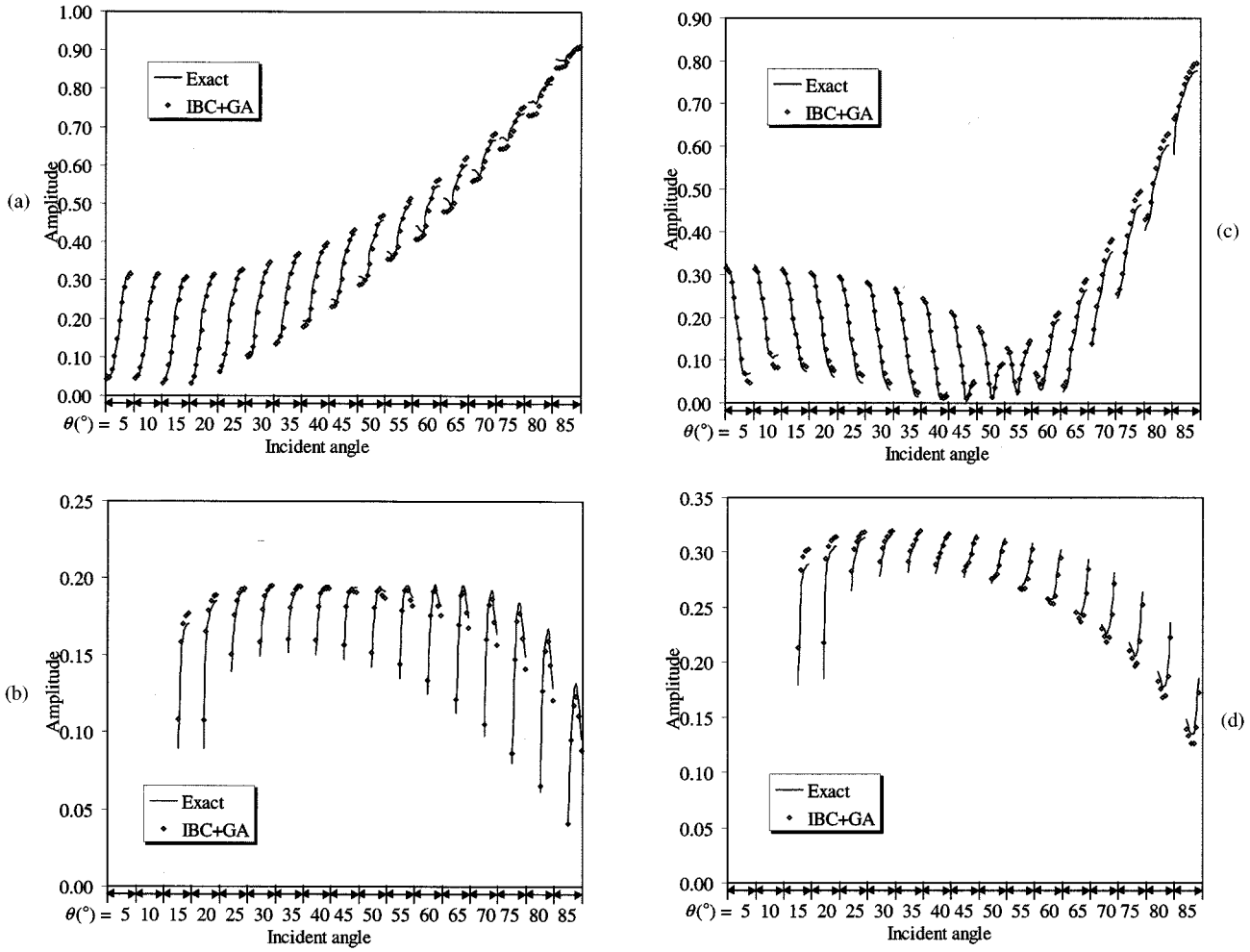

Fig. 8. Higher order reflection coefficients simulated by the IBC model. (a) 0th order, H-pol. (b) First order, H-pol. (c) 0th order, V-pol. (d) 1st order, V-pol.

where c_1 and c_2 are constants and C_i is the ith chromosome in the population. This fitness value is used in ranking the chromosomes and selecting of parents for the next generation [8]–[11]. There are several standard ways of selection. In this paper, the roulette wheel selection is used in which the probability of each chromosome to be selected is proportional to its fitness value.

After two chromosomes are selected, they mate to generate children. This is realized by the process of crossover in which a break point is randomly chosen in the chromosomes and the two chromosomes are switched at that point. Mutation is imposed at this point so that new genes appear in the next generation. The mutation rate, which is the portion of bits to be randomly changed, is also an important parameter in GA. Experiments show that a mutation rate of 5–8% is often efficient in the calculation.

The process of evaluation, selection, and reproduction is repeated until a desired mean-squared error is achieved or a maximum generation is reached. For a population of 400 chromosomes, the 0th order IBC (i.e., $N = 0$) takes 10–20 generations to converge to the optimum while the second-order IBC takes 200–400 generations.

III. Numerical Examples

In this section, some examples are presented to demonstrate the effectiveness of the method. The first example is a deep triangular grooved grating with relatively small period. The geometry of one cell of the grating is shown in Fig. 4(a) where the period $p = 0.067\lambda_0$ and $h_1 = 0.22\lambda_0, h_2 = 0.017\lambda_0$. The coating material is MagRAM with material constants $\varepsilon_r = 14.35 - j0.28$ and $\mu_r = 1.525 - j1.347$ at the frequency of 10 GHz. Seventeen observation angles are selected which include normal incidence and the combination of $\theta = 20^\circ, 40^\circ, 60^\circ, 80^\circ$ and $\phi = 0^\circ, 30^\circ, 60^\circ, 90^\circ$. In this example, we set Z_{xx} and Z_{zz} in (1) to zero and $N = 0$ in (4) to make the model comparable with TIBC. The co-polarization reflection coefficients for the H-pol and V-pol incidence are plotted in Fig. 5(a) and (b), respectively, and the H–V cross-polarization reflection coefficients are plotted in Fig. 5(c). In the figures, the x-axis is divided into sections of different incident angle θ, which varies from 5° to 85° in steps of 10°. In each of the θ section, the grating angle ϕ varies from 0° to 90°. The matching of the reflection coefficients between the GA approach and MoM solution is good at most incident angles, even near grazing incidence. The value of

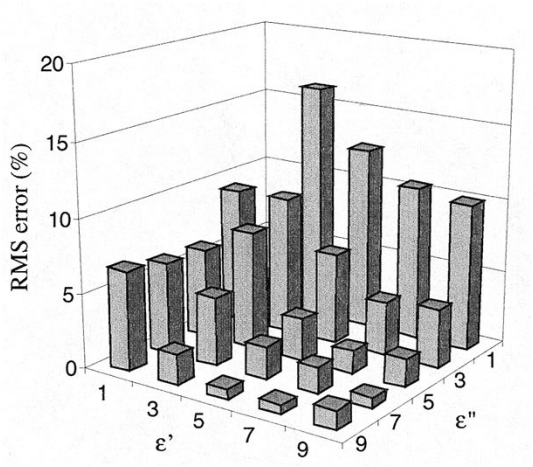

Fig. 9. Error of the IBC model as a function of material constant $\varepsilon = \varepsilon' - j\varepsilon''$.

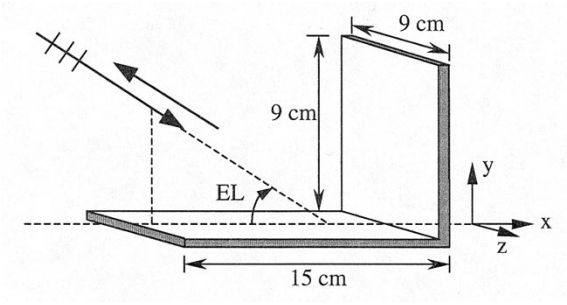

Fig. 10. Geometry of the corner reflector.

d is found to be $0.027\lambda_0$ from the tip of the groove or $0.21\lambda_0$ above the ground plane. The TIBC result is also generated by using the reflection coefficient at normal incidence to derive the equivalent boundary condition. The impedance surface is placed at the plane of the conductor backing. It can be seen that the TIBC results deviate significantly from the reference solution away from normal incidence. With the same complexity of the boundary condition, GA achieves a much better matching because more observation points are used in the modeling and because of the additional degree of freedom in the position of the IBC surface.

Next, we compare the IBC approximations with and without the cross impedance terms Z_{xx} and Z_{zz}. The structure is a rectangular groove as shown in Fig. 4(b) with a period $p = 0.17\lambda_0$ and a groove depth of $h_1 = h_2 = 0.042\lambda_0$. The material constants are $\varepsilon_r = 8.3 - j2.4$ and $\mu_r = 2 - j0.9$ at 10 GHz. The same observation points are used as in the previous example. The 0th order $(N = 0)$ IBC is determined and the comparison between the reflection coefficients is illustrated in Fig. 6. With the cross impedance included, the accuracy of the approximation is improved.

In the third example, the IBC of different orders are obtained for the structure shown in Fig. 4(b) where $p = 0.42\lambda_0, h_1 = 0.25\lambda_0$ and $h_2 = 0.17\lambda_0$. The coating material is the same as that in example 2 but the period is much larger and the groove is deeper. The reflection coefficients predicted by the 0th-order and second-order model are plotted in Fig. 7. While the approximation by the 0th-order model is fairly satisfactory, the second-order model further improves the result and the matching is better at most incident angles. The price of the improvement is the computation time. For the 0th-order modeling, it takes only a few minutes for the GA to converge while the second-order IBC takes more than 1 h on an SGI O2 workstation (R10000/155 MHz). Another consequence as the order of the model is increased is that the resulting IBC will show more spatial variation. This implies that when the IBC model is utilized in subsequent analysis using numerical electromagnetics solvers, the impedance surface must be divided more finely to faithfully describe the IBC. This will lead to a higher computation cost. Thus, the higher order model is not recommended unless the 0th-order one is intolerable or the period is large compared to the wavelength. Generally speaking, the IBC model can be improved by increasing the model order whether or not the cross-impedance terms exist. But with the cross-impedance terms, the required model order is usually smaller than that without them.

We further investigate a structure with a period larger than half a wavelength, which results in higher order Floquet-mode reflection at some incident angles. The rectangular groove shown in Fig. 4(b) has a period $p = 0.85\lambda_0$ and $h_1 = h_2 = 0.42\lambda_0$. The material constant are $\varepsilon_r = 10.5 - j2.2$ and $\mu_r = 2 - j0.3$. The 0th and 1st order reflection coefficients are plotted in Fig. 8(a) and (b), respectively. It is shown that the Floquet modes are also well characterized.

In the final example, we investigate the limitation of the IBC model. We consider a triangular groove shown in Fig. 4(a) with $p = 0.33\lambda_0$ and $h_1 = h_2 = 0.08\lambda_0$. The optimal IBC model is found using the GA for different coating materials. A second-order IBC model with cross impedance terms is used and the optimal model parameters are determined by running GA to convergence. After the model is found, the root mean squared (RMS) error of the IBC-predicted reflection coefficients over the selected angles are computed. Fig. 9 shows the RMS error of the optimal IBC model as a function of ε_r' and ε_r'', which are the real and imaginary parts of the coating relative permittivity ε_r. μ_r is set to one for all the coatings. We observe that the IBC model works best for high-contrast high-loss materials. For low-contrast or low-loss materials, the model error can be large. This behavior is very similar to conventional IBC models for planar coatings.

We now apply our derived IBC model to a three-dimensional (3-D) scattering problem. Consider the corner reflector as shown in Fig. 10. The monostatic radar cross section (RCS) is calculated for both the uncoated reflector and that coated with the MagRAM structure described in example 1. The groove of the coating is either parallel or perpendicular to the incident direction. Both cases are computed for comparison. Note that the solution for such a structure is very complicated if we try to use the exact MoM formulation. Instead, we use the 0th-order impedance boundary condition obtained from example 1 to replace the corrugated

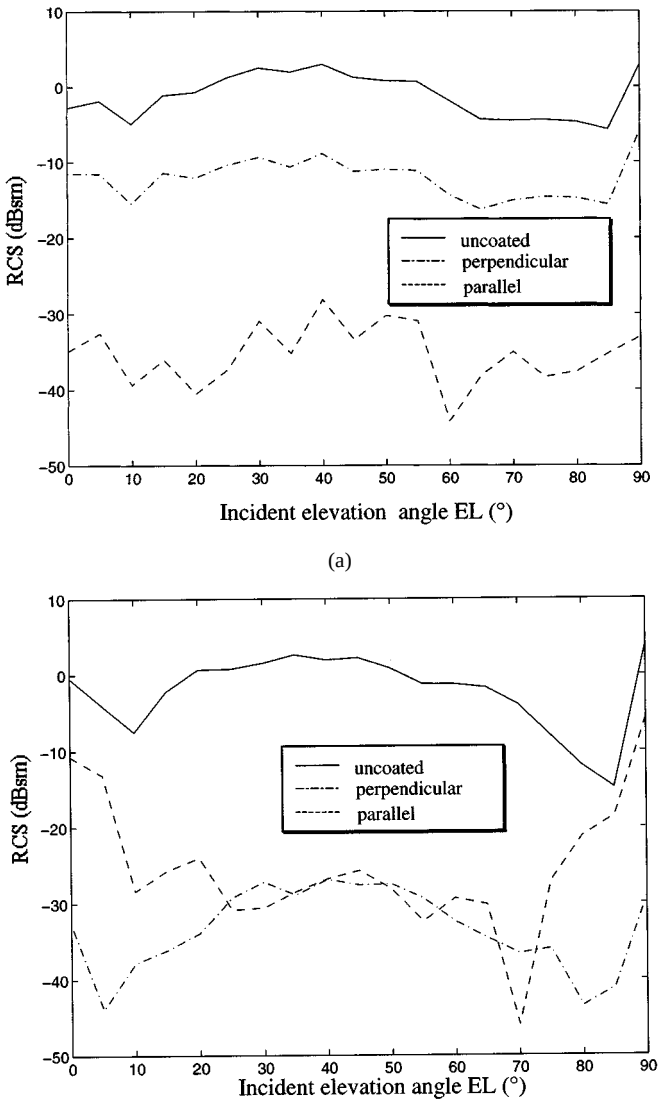

Fig. 11. RCS of the corner reflector ($f = 10$ GHz). (a) H-polarization. (b) V-polarization.

absorber. We assume that the size of the plate remain the same after the IBC replacement. The RCS is computed using FISC [12], which is a 3-D MoM code based on the fast multipole method [13]. Comparisons of the RCS at several elevation angles are shown in Fig. 11 for both the H- and V-polarizations. The result shows the effect of coating, which lowers the overall RCS level for both polarizations. We further observe that a 30-dB RCS reduction can be achieved for both polarizations over the range of elevation angles from 20° to 75° if the grating is oriented parallel to the incident wave.

IV. Conclusion

In this paper, an impedance boundary condition model is derived based on the GA to approximate arbitrary corrugated coating structures in scattering problems. The periodic structure is replaced by a periodic IBC on a virtual surface. The boundary impedance and the position of the surface are optimized by matching the reflection coefficients to the rigorous numerical solution at a number of incident angles. Similar to traditional IBC models, this approach is most effective when the coating material is high loss and of high contrast. The resulting IBC model generated by this algorithm can be incorporated into an existing computational electromagnetics code to assess the performance of the corrugated coating when mounted on complex platforms.

Compared with other IBC approaches, the method described above has several advantages. First, the boundary impedance is assumed to be anisotropic so that the same model can be applied to oblique incidence from any arbitrary angles. Second, it is possible to build in spatial variation of the boundary impedance by adjusting the number of terms used in the Fourier series expansion. By using more terms, the IBC model can be made more accurate. In addition, the position of the impedance surface can also be optimized. By solving for the best position of the impedance surface as one of the model parameters, the accuracy of the model can be improved.

Numerical experiments show that the IBC approximation can be improved if some of the parameters of the GA are carefully chosen. These parameters include the incident angles at which the rigorous solution is obtained, the range of each model parameter, and the mutation rate, etc. The GA can also be accelerated with carefully chosen parameters and a well-designed cost function.

References

[1] D. J. Hoppe and Y. Rahmat-Samii, *Impedance Boundary Conditions in Electromagnetics*. Bristol, PA: Taylor Francis, 1995.
[2] T. B. A. Senior and J. L. Volakis, *Approximate Boundary Conditions in Electromagnetics*. London, U.K.: Inst. Elect. Eng., 1995.
[3] G. Pelosi and P. Y. Ufimtsev, "The impedance-boundary condition," *IEEE Antennas Propagat. Mag.*, vol. 38, pp. 31–34, Feb. 1996.
[4] T. B. A. Senior and J. L. Volakis, "Derivation and application of a class of generalized boundary conditions," *IEEE Trans. Antennas Propagat.*, vol. 37, pp. 1566–1572, Dec. 1989.
[5] K. W. Whites and R. Mittra, "Equivalent boundary-condition model for lossy planar periodic structures at low frequencies," *IEEE Trans. Antennas Propagat.*, vol. 44, pp. 1617–1629, Dec. 1996.
[6] J. Moore, H. Ling, and C. S. Liang, "The scattering and absorption characteristics of material-coated periodic grating under oblique incidence," *IEEE Trans. Antennas Propagat.*, vol. 41, pp. 1281–1288, Sept. 1993.
[7] R. Petit, Ed., *Electromagnetic Theory of Gratings*. New York: Springer-Verlag, 1980.
[8] *Handbook of Genetic Algorithms*, L. Davis, Ed., Van Nostrand Reinhold, New York, 1991.
[9] R. L. Haupt, "An introduction to genetic algorithms for electromagnetics," *IEEE Antennas Propagat. Mag.*, vol. 37, pp. 7–15, Apr. 1995.
[10] D. S. Weile and E. Michielssen, "Genetic algorithm optimization applied to electromagnetics: A review," *IEEE Trans. Antennas Propagat.*, vol. 45, pp. 343–353, Mar. 1997.
[11] G. Winter, J. Periaux, M. Galan, and P. Cuesta, *Genetic Algorithms in Engineering and Computer Science*. New York: Wiley, 1995.
[12] User's Manual for FISC (Fast Illinois Solver Code), Ctr. Computat. Electromagn., Univ. Illinois and DEMACO, Champaign, IL, Jan. 1997.
[13] J. M. Song and W. C. Chew, "Fast multipole method solution using parametric geometry," *Microwave Opt. Tech. Lett.*, vol. 7, pp. 760–765, Nov. 1994.

Tao Su (S'97) was born in Beijing, China, in 1973. He received the B.S. degree in electronics engineering from Tsinghua University, Beijing, in 1996, and the M.S. degree in electrical engineering from the University of Texas at Austin in 1997. He is currently working toward the Ph.D. degree at the University of Texas at Austin.

Since 1996, he has been working as a Graduate Research Assistant in the Department of Electrical and Computer Engineering, University of Texas at Austin. His research interests include simulation and modeling of antenna-platform radiation, model based parameter estimation in scattering and radiation problems, optimization methods in computational electromagnetics, and the coupling effect in array signal processing.

Hao Ling (S'83–M'86–SM'92–F'99) was born in Taichung, Taiwan, on September 26, 1959. He received the B.S. degrees in electrical engineering and physics from the Massachusetts Institute of Technology, Cambridge, in 1982, and the M.S. and Ph.D. degrees in electrical engineering from the University of Illinois at Urbana-Champaign, in 1983 and 1986, respectively.

In September 1986, he joined the faculty of the University of Texas at Austin and is currently a Professor of electrical and computer engineering. In 1982 he was associated with the IBM Thomas J. Watson Research Center, Yorktown Heights, NY, where he conducted low-temperature experiments in the Josephson Program. He participated in the Summer Visiting Faculty Program in 1987 at the Lawrence Livermore National Laboratory, CA. In 1990 he was an Air Force Summer Fellow at the Rome Air Development Center, Hanscom Air Force Base, MA. His research interests are in radar signature prediction, computational techniques, and radar signal analysis for scattering mechanism interpretation and target identification.

Dr. Ling was a recipient of the National Science Foundation Presidential Young Investigator Award in 19987, the NASA Certificate of Appreciation in 1991, and the Archie Straiton Junior Faculty Teaching Excellence Award in 1993 and holder of the Chevron Centennial Fellowship in Engineering.